AJ, IN PRESS
Preprint typeset using LaTeX style emulateapj v. 08/22/09

arXiv:0810.0682v1 [astro-ph] 3 Oct 2008

THE GLOBULAR CLUSTER NGC 5286. I. A NEW CCD *BV* COLOR-MAGNITUDE DIAGRAM

M. ZOROTOVIC,[1] M. CATELAN,[1] M. ZOCCALI[1] B. J. PRITZL,[2] H. A. SMITH,[3]
A. W. STEPHENS,[4] R. CONTRERAS,[1,5] M. E. ESCOBAR[1]

AJ, in press

ABSTRACT

We present *BV* photometry of the Galactic globular cluster NGC 5286, based on 128 *V* frames and 133 *B* frames, and covering the entire face of the cluster. Our photometry reaches almost two magnitudes below the turn-off level, and is accordingly suitable for an age analysis. Field stars were removed statistically from the cluster's color-magnitude diagram (CMD), and a differential reddening correction applied, thus allowing a precise ridgeline to be calculated.

Using the latter, a metallicity of [Fe=H] = $-1.70 \quad 0.10$ in the Zinn & West scale, and [Fe=H] = $-1.47 \quad 0.02$ in the Carretta & Gratton scale, was derived on the basis of several parameters measured from the red giant branch, in good agreement with the value provided in the Harris catalog.

Comparing the NGC 5286 CMD with the latest photometry for M3 by P. B. Stetson (2008, priv. comm.), and using VandenBerg isochrones for a suitable chemical composition, we find evidence that NGC 5286 is around $1.7 \quad 0.9$ Gyr older than M3. This goes in the right sense to help account for the blue horizontal branch of NGC 5286, for which we provide a measurement of several morphological indicators. If NGC 5286 is a bona fide member of the Canis Major dwarf spheroidal galaxy, as previously suggested, our results imply that the latter's oldest components may be at least as old as the oldest Milky Way globular clusters.

Subject headings: stars: Hertzsprung-Russell diagram — stars: variables: other — Galaxy: globular clusters: individual (NGC 5286, NGC 5272) — galaxies: dwarf — galaxies: star clusters

1. INTRODUCTION

Globular clusters (GCs) are among the very oldest objects in the Universe. Accordingly, detailed studies of their stellar contents, including both the variable and non-variable components, hold the key to the formation and early evolution of galaxies – and of our own Galaxy in particular. RR Lyrae variable stars, which are present in GCs in large numbers (e.g., Clement et al. 2001), play a particularly important role in determining the extent to which the Galaxy may have formed from the accretion of smaller "protogalactic fragments," as currently favored by CDM cosmology (e.g., Catelan 2005, 2007). However, while over 150 Galactic GCs are currently known (see, e.g., Borissova et al. 2007, and references therein), only a relatively small fraction has been surveyed for stellar variability using state-of-the-art techniques, including CCD detectors and image subtraction algorithms. We have accordingly started an extensive variability survey of GCs (e.g., Catelan et al. 2006), with the ultimate goal to help put constraints on the way the Galaxy has formed. As a natural by-product of our variability searches, deep and high-precision color-magnitude diagrams (CMDs) are obtained, often covering large areas over the face of the observed clusters. This affords a new look into the clusters' physical parameters, as implied by these CMDs.

NGC 5286 (C1343-511) is a particularly interesting object in this context. This is a bright ($M_V = -8.26$) and fairly compact GC (with a core radius of 0.29^0, a half-light radius of only 0.69^0, and a tidal radius of 8.36^0), of intermediate metallicity ([Fe=H] = -1.67) in Centaurus (all values from Harris 1996). It may be associated with the Canis Major dwarf spheroidal galaxy (Frinchaboy et al. 2004; see also Forbes, Strader, & Brodie 2004). Unfortunately, NGC 5286 has received relatively little attention, the latest studies to produce a CMD having been the one by Samus et al. (1995), which relied on a CCD with $512 \quad 320$ pixels^2, covering a field of view of only $3.1 \quad 1.9$ arcmin^2, and avoiding the cluster center; and the one by Brocato et al. (1996), which – though covering a larger area over the face of the cluster – did not produce a sufficiently deep CMD as to provide a reliable ridgeline extending below the main-sequence (MS) turnoff (TO) point (see their Fig. 8). One of the reasons for the relative neglect of this cluster may have been its relatively high foreground reddening, $E(B-V) = 0.24$ (Harris 1996). In the same vein, NGC 5286 has never been properly studied, using state-of-the-art techniques, in terms of its variable star content, even though it is known to harbor over a dozen RR Lyrae variables (e.g., Clement et al. 2001).

The main purpose of the present study is to provide the first extensive, CCD-based variability study of NGC 5286, which leads to a deep CMD covering a much larger field over the face of the cluster than has been available thus far. In the present paper we shall report on the CMD and the derived cluster parameters, whereas a companion paper (Zorotovic et al. 2008, hereafter Paper II) will describe in detail the variability search and derived variable star parameters for the 56 variables that were found in NGC 5286 (which increases by a

BASED ON OBSERVATIONS OBTAINED WITH THE 1.3M WARSAW TELESCOPE AT THE LAS CAMPANAS OBSERVATORY, CHILE.

[1] Pontificia Universidad Católica de Chile, Departamento de Astronomía y Astrofísica, Av. Vicuña Mackenna 4860, 782-0436 Macul, Santiago, Chile; e-mail: mzorotov, mcatelan, mzoccali, mescobar@astro.puc.cl

[2] Department of Physics and Astronomy, University of Wisconsin Oshkosh, Oshkosh, WI 54901; e-mail: pritzlb@uwosh.edu

[3] Department of Physics and Astronomy, Michigan State University, East Lansing, MI 48824; e-mail: smith@pa.msu.edu

[4] Gemini Observatory, 670 N. Aóhoku Place, Hilo, HI 96720; e-mail: astephens@gemini.edu

[5] Current address: INAF, Osservatorio Astronomico di Bologna, via Ranzani 1, I-40127 Bologna, Italy; e-mail: rodrigo.contreras@oabo.inaf.it

factor of 3 the number of known/measured variables in the cluster).

We begin in §2 by describing the acquired data and reduction techniques. In §3 we describe our derived CMD, along with the physical parameters of the cluster obtained therefrom. §4 is devoted to a differential age comparison with M3, a cluster of similar metallicity to NGC 5286. We finally close in §5 by summarizing the results of our investigation.

2. OBSERVATIONS AND DATA REDUCTION

Time-series B, V images of NGC 5286 were collected over a one-week run in April 2003, with the 1.3m Warsaw University Telescope at Las Campanas Observatory (LCO) and using the "second generation" CCD mosaic camera, commisioned in May 2001. The 8kMOSAIC camera consists of eight thin SITe 2048 4096 CCD chips (8192 8192 pixels of 0.26 arcsec/pixel), giving a total field of view equal to 35^0 35^0. The readout time of the camera is 98 seconds, with readout noise of 6 to 9 e^- (depending on the chip) and gain of 1.3 e^-/ADU. A total of 128 frames in V and 133 frames in B were thus acquired.

In this work we present the results for chip 2, covering a field of 9^0 17^0, where the cluster dominates. We use chip 3, covering a similar field, to select field stars to perform statistical decontamination of the cluster.

Photometry was performed using DAOPHOT II/ALLFRAME (Stetson 1987, 1994). Our calibration is the same as presented by Contreras et al. (2005) and Contreras et al. (2008, in preparation) in their study of M62 (NGC 6266), and by Escobar et al. (2008, in preparation) in their study of M69 (NGC 6637). These two clusters were observed during the same nights, and with the same telescope/instrument combination, as NGC 5286. To obtain the employed calibration, several different Landolt (1992) fields were observed during photometric nights, including PG+0918, PG+1323, PG+1525, PG+1528, PG+1633, PG+1657, and RU 152. These fields were centered on chip 2, where most of the stars in the observed clusters were found. A total of 117 and 157 Landolt standard stars in B and V, respectively, were used to derive our final calibrations. The derived equations for B and V had root-mean-square deviations of order 0.18 mag in B and 0.04 mag in V. The derived calibration was then propagated to chip 3, by using about 660 stars in common between chips 2 and 3. Further details of the derived calibrations will be provided in Contreras et al. (2008) and Escobar et al. (2008).

3. COLOR-MAGNITUDE DIAGRAM

3.1. *Field-Star Decontamination*

Our derived CMD for the main cluster field (chip 2), after removing the innermost cluster regions (r 0.3^0) which are badly affected by crowding, is shown in Figure 1 (*left panel*). Known variables (see Paper II) were removed from this CMD. As can be seen, field contamination is not negligible, which may adversly affect our determination of the cluster ridgeline, and thus the measurement of key physical parameters for the cluster (including its age and metallicity). We have accordingly resorted to performing a statistical decontamination of the observed CMD, using the method described in Gallart et al. (2003), with a maximum distance $d = 0.15$ mag.

We use as control field the stars from chip 3 that lie outside the tidal radius; their corresponding CMD is shown in Figure 1 (*right panel*). Figure 2 shows the resulting (B–V,V) CMD, after decontamination. As can be seen from this figure, the main branches still reveal some spread, which does not decrease substantially as one goes towards brighter magnitudes – as would have been expected if it were due to photometric errors alone. We therefore suspect that a small amount of differential reddening may be the culprit. To check this, we have mapped the cluster CMD following the procedure described, e.g., in Piotto et al. (1999). Indeed, Figure 3 shows that different regions of chip 3 yield CMDs that are shifted, with respect to a reference mean locus, along the reddening vector. It does appear, therefore, that differential reddening is present in NGC 5286, at the level of a few hundredths of a magnitude in $E(B–V)$.

To produce a tighter CMD, a correction was applied to minimize this effect, following the procedure described in Piotto et al. (1999). The resulting CMD is shown in Figure 4. Due to the saturation of points in this plot, the difference is not so

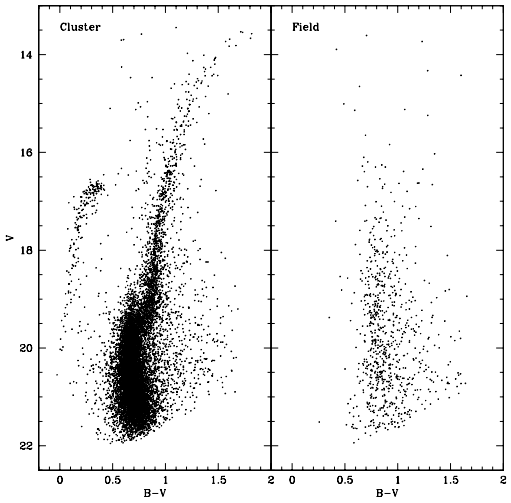


FIG. 1.— *Left*: (B–V,V) CMD for NGC 5286 before field-star decontamination. The innermost cluster regions (r 0.3^0) are not shown. *Right*: (B–V,V) CMD for field stars used to carry out the decontamination.

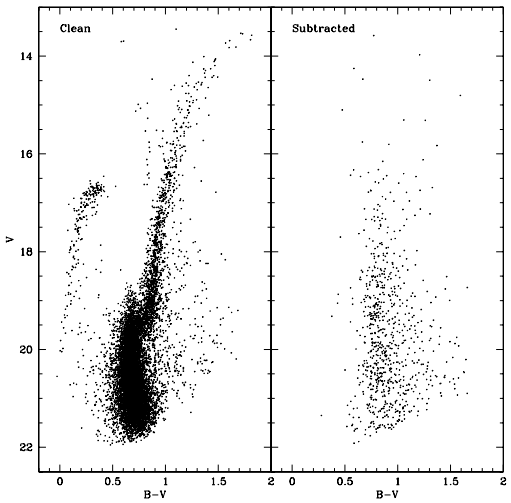


FIG. 2.— *Left:* The CMD of NGC 5286, after statistical decontamination from field stars. *Right:* Stars subtracted from the original CMD (Fig. 1, left) in order to obtain the decontaminated CMD shown on the left.

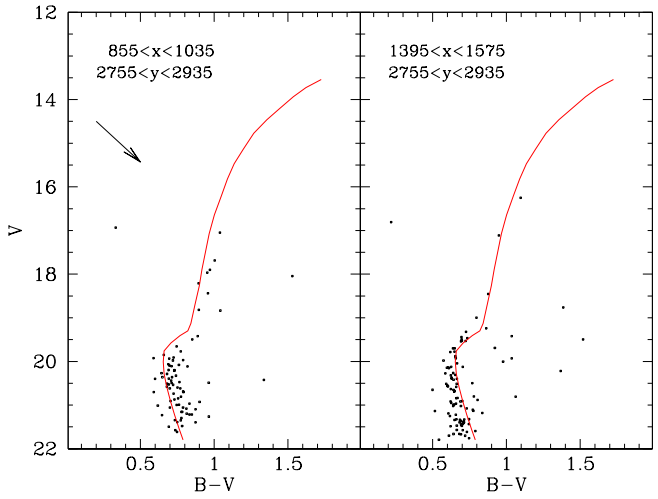


FIG. 3.— Examples of CMDs for two small areas located in different regions across the face of the cluster (*see labels*). Clearly, the two CMDs are shifted along the reddening vector (shown by the arrow) with respect to the reference mean locus, indicating the presence of differential reddening across the face of the cluster.

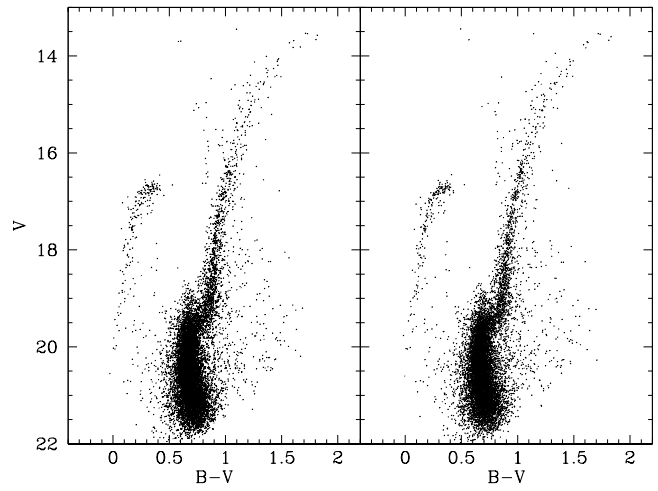


FIG. 4.— Comparison between the original, decontaminated cluster CMD (*left*) and the one corrected for differential extinction across the cluster area (*right*).

striking in the MS, while the red giant branch (RGB) and the blue horizontal branch (HB) do appear significantly narrower.

Finally, in order to further improve the CMD, stars with too large errors in both B and V were excluded. As shown in Figure 5, the applied error cut follows the shape of the lower envelope of the error distribution (Poisson error), thus excluding the stars with large errors *compared* to the error expected at their respective magnitude levels. The resulting CMD is shown in the right panel of Figure 5. This is our final CMD for the cluster, and the one used in the subsequent analysis.

Before proceding, we note that our CMD is clearly in good qualitative agreement with the ones previously published by Samus et al. (1995) and Brocato et al. (1996), revealing a predominantly blue HB and a moderately steep RGB indicative of an intermediate-to-low metallicity.

To determine the mean ridgelines, we have experimented with several different techniques, but finally decided upon what essentially amounts to an eye fit to the data, similar

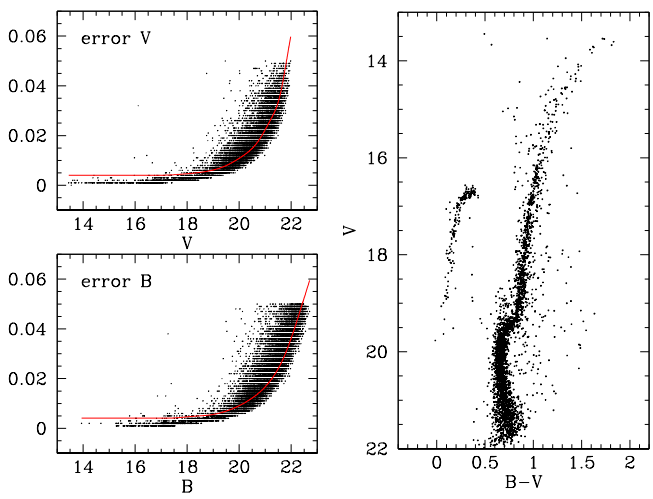


FIG. 5.— Selection based on the photometric errors (*left*), and final CMD for NGC 5286 (*right*).

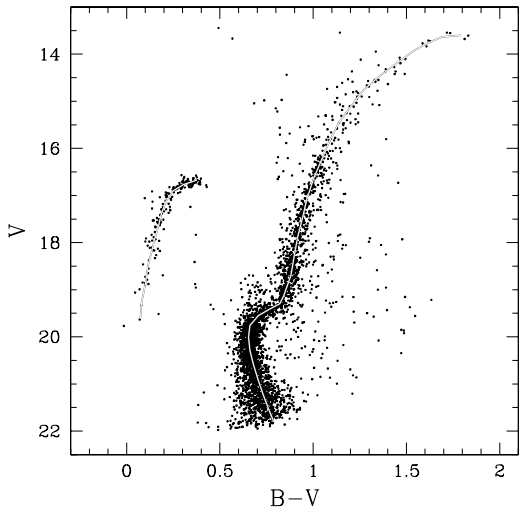


FIG. 6.— (B–V,V) CMD for NGC 5286, with the derived ridgelines overplotted.

to the procedure previously followed, for instance, by Bedin et al. (2000) and Stetson, Catelan, & Smith (2005). Table 1 presents the adopted normal points for each branch. In Figure 6 the (B–V,V) CMD is shown with the mean ridgelines overplotted.

To determine the position of the turn off we fit a parabola to a small region of the MS near the TO point. The MS TO point is found to be at V_{TO} = 20.05 ± 0.01 mag and (B–V) = 0.66 ± 0.02.

3.2. *Metallicity and Reddening*

Ferraro et al. (1999, hereafter F99) derived a set of metallicity indicators in terms of RGB parameters. We use equations from Table 4 in F99 to estimate the metallicity for NGC 5286 in the Carretta & Gratton (1997, hereafter CG97) scale, [Fe/H]$_{CG97}$, and the global metallicity, [M/H]. The latter takes into due account the effects of an enhancement in the abundance of the so-called -capture elements with respect to the solar proportions (e.g., Salaris, Chieffi, & Straniero 1993).

TABLE 1
MEAN FIDUCIAL POINTS FOR NGC 5286

V	$(B-V)$
MS + SGB[a] + RGB	
13.602	1.793
13.636	1.692
13.785	1.602
13.933	1.537
14.213	1.441
14.464	1.356
14.771	1.268
15.135	1.197
15.470	1.136
15.819	1.090
16.210	1.048
16.643	1.002
17.076	0.966
17.495	0.941
17.886	0.917
18.263	0.899
18.696	0.880
19.129	0.842
19.297	0.821
19.409	0.768
19.546	0.707
19.758	0.661
20.009	0.654
20.288	0.661
20.582	0.679
20.903	0.704
21.224	0.732
21.560	0.764
21.797	0.789
Blue HB	
16.671	0.378
16.769	0.303
16.908	0.247
17.118	0.211
17.383	0.186
17.635	0.172
17.914	0.150
18.207	0.133
18.487	0.115
18.864	0.101
19.283	0.080
19.618	0.073

[a] SGB = subgiant branch.

Since several of these indicators require a precise definition of the HB level, before proceeding we must first determine the HB level in the same way as in F99. These authors adopt for the HB the zero-age HB (ZAHB) level in their measurements. The latter is defined as the magnitude of the lower envelope of the observed HB distribution in the region with $0.2 < (B-V)_0 < 0.6$. As we do not have many non-variable stars in this region, we decided to use a theoretical ZAHB (from VandenBerg, Bergbusch, & Dowler 2006, for a chemical composition [Fe/H] = −1.71, [/Fe] = 0.3) to match the lower envelope of the HB distribution. We use a reddening of $E(B-V) = 0.24$ (Harris 1996) and we vertically shifted the simulated ZAHB to match the lower envelope of the observed HB, arriving at the best match that is shown in Figure 7. The average ZAHB magnitude over the quoted color range provides us with our final $V_{\rm ZAHB} = 16.69$.

For NGC 5286, we used the mean ridgeline to measure the following RGB parameters: $(B-V)_{0g}$ (RGB color at the HB level); $V_{1.1}$, $V_{1.2}$, and $V_{1.4}$ [magnitude difference between the HB and RGB at fixed colors $(B-V)_0 = 1.1$, 1.2, and 1.4, respectively]; and the two RGB slopes $S_{2.5}$ and $S_{2.0}$ (slope of the line connecting the intersection of the RGB and HB with the points along the RGB located 2.0 and 2.5 mag brighter than the HB, respectively).

TABLE 2
NGC 5286 METALLICITY

Parameter	[Fe/H]$_{\rm CG97}$	[M/H]]
$(B-V)_{0g} = 0.762$	−1.48	−1.27
$V_{1.1} = 2.154$	−1.48	−1.28
$V_{1.2} = 2.470$	−1.46	−1.27
$V_{1.4} = 2.950$	−1.44	−1.24
$S_{2.5} = 5.648$	−1.50	−1.25
$S_{2.0} = 6.903$	−1.47	−1.26
Mean	−1.47 0.02	−1.26 0.02

To infer the metallicity from these indices, colors had first to be corrected by extinction. In the Feb. 2003 edition of the Harris (1996) catalog, a value $E(B-V) = 0.24$ is provided. For comparison, on the basis of the Schlegel, Finkbeiner, & Davis (1998) dust maps one finds $E(B-V) = 0.292$ mag. However, for high reddening values there is some indication that the Schlegel et al. maps may overestimate the reddening value. Using equation (1) in Bonifacio, Monai, & Beers (2000) to correct for this, one gets a corrected reddening value of $E(B-V) = 0.225$ mag. While Zinn (1985) gives an $E(B-V) = 0.27$ mag for the cluster, Webbink (1985) gives instead $E(B-V) = 0.21$ mag. Reed, Hesser, & Shawl (1988), on the other hand, list two possible reddening values for the cluster, namely $E(B-V) = 0.28$ mag and $E(B-V) = 0.24$ mag. Taking a straight average over all the quoted values (except the high original value from the Schlegel et al. maps), one finds for NGC 5286 a suggested average value of $E(B-V)$ ′ 0.24 0.03. We shall accordingly assume $E(B-V) = 0.24$ for NGC 5286.

The individual metallicity values derived from each of the indices defined above are listed in Table 2.[6] A median over the listed results gives for NGC 5286 a metallicity [Fe/H]$_{\rm CG97}$ = −1.47 0.02 and [M/H] = −1.26 0.02 (standard deviation of the mean). That give us a value of [Fe/H] = −1.70 0.10 in the Zinn & West (1984, hereafter ZW84) scale, in good agreement with Harris (1996).

As a check of the adopted reddening and metallicity values, we have also applied the simultaneous reddening and metallicity (SRM) method of Sarajedini (1994), as ported to the V, $B-V$ plane by F99. The slopes $S_{2.5}$ and $S_{2.0}$ do not depend on the reddening. Using the average values of [Fe/H] and [M/H] based only on these two slopes, we obtain $(B-V)_{0g} = 0.761$ and $(B-V)_{0g} = 0.765$, respectively – in excellent agreement with the values found in Table 2. We conclude that the assumed reddening value of $E(B-V) = 0.24$ mag must be close to the correct value for the cluster.

3.3. *Horizontal Branch Morphology*

Figure 7 shows the HB region of the NGC 5286 CMD in the $(B-V,V)$ plane. As before, known variable stars were omitted from this plot (see Paper II for a detailed discussion of the NGC 5286 variable star content).

We computed useful HB morphology parameters like the *Lee-Zinn parameter* L (Zinn 1986; Lee 1990; Lee, Demarque, & Zinn 1990) and the *Buonanno parameter* P_{HB} (Buonanno 1993; Buonanno et al. 1997), defined as

[6] Note that equation (4.6) in F99 actually calibrates $S_{2.0}$ in terms of [M/H], whereas their equation (4.13) calibrates the same quantity in terms of [Fe/H] – and not the other way around, as incorrectly stated in their paper. We thank F. Ferraro for his help in clarifying this point.

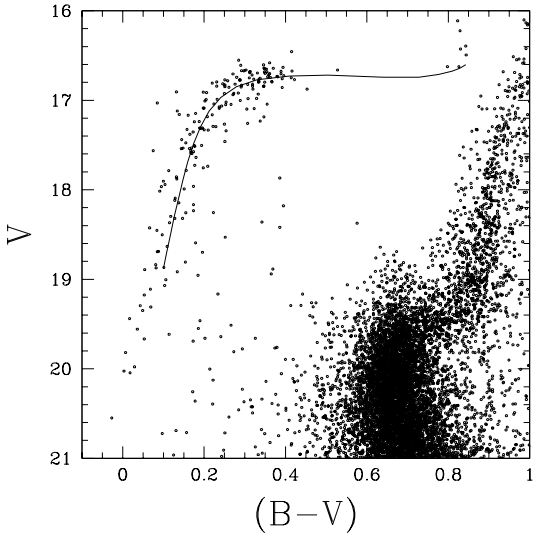


FIG. 7.— Zoomed NGC 5286 CMD around the HB region with VandenBerg et al. (2006) ZAHB for [Fe/H] = −1.71, [/Fe] = 0.3)

$$L \quad (B-R)/(B+V+R); \tag{1}$$

$$P_{HB} \quad (B2-R)/(B+V+R); \tag{2}$$

where B2 is the number of blue HB stars bluer than $(B-V)_0 = -0.02$, and B, V, R are the numbers of blue, variable (RR Lyrae), and red HB stars, respectively. We also derived two parameters defined by Preston, Schectman, & Beers (1991): the mean unreddened color of blue HB between $-0.02 < (B-V)_0 < 0.18$, $(B-V)_W$, and the number of HB stars in this color interval normalized by the number of HB stars with $(B-V)_0 < 0.18$, B_W/B. Table 3 shows the HB morphology parameters for NGC 5286.

TABLE 3
HB MORPHOLOGY PARAMETERS FOR NGC 5286

Parameter	Value
B : V : R	0.764 : 0.338 : 0.027
B/(B+R)	0.973 0.03
(B−R)/(B+V+R)	0.739 0.02
(B2−R)/(B+V+R)	0.342 0.02
$(B-V)_W$	0.074 0.005
B_W/B	0.523 0.05

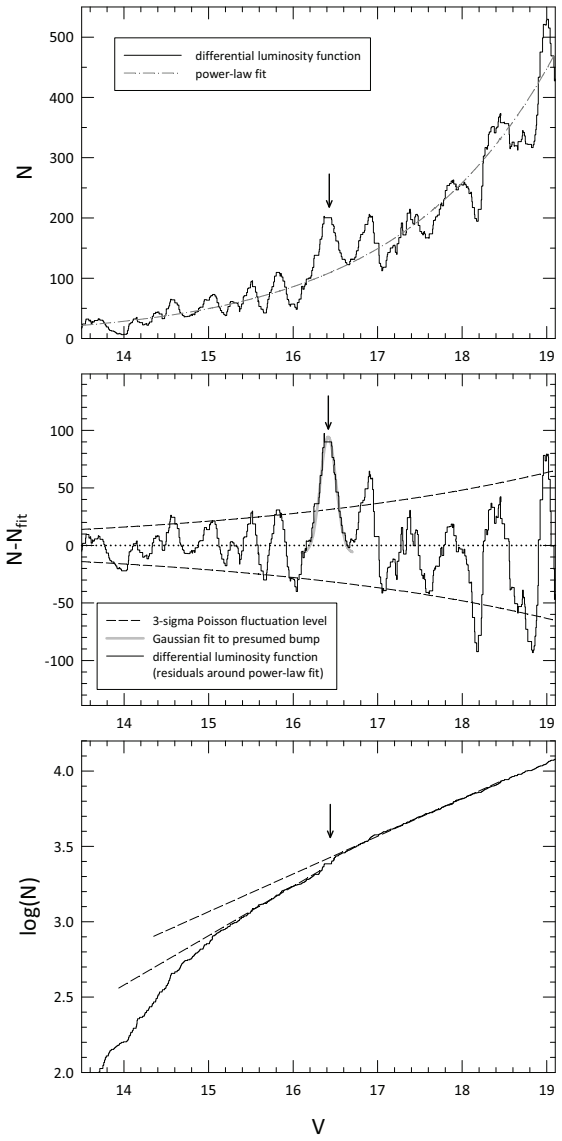


FIG. 8.— *Top*: differential RGB luminosity function for NGC 5286 (*solid line*). A power-law fit to the data is shown as a *dash-dotted gray line*. *Middle*: the residuals around the power-law fit are shown as a *solid line*. The *dashed lines* indicate the Poisson 3− level, as computed based on the derived power-law fit. The gray line shows the Gaussian fit over a 0.3 mag region around the candidate RGB bump peak. *Bottom*: cumulative luminosity function, indicating the break expected if the bump is present at the indicated location. All three panels consistently indicate that the RGB bump is located at the position marked by the arrow.

3.4. *Red Giant Branch*

During the RGB phase, the H-burning shell advances outward in mass, leading to a continued increase in mass of the He core. Eventually, the H-burning shell actually encounters the chemical composition discontinuity that was left behind as a consequence of the maximum inward penetration of the convective envelope. Since the envelope is naturally H-rich, this means that the H-burning shell is suddenly presented with an extra supply of fuel. The structure of the star, presented with this extra fuel supply, readjusts momentarily to this new situation, with an actual (small) reversal in its direction of evolution before it resumes its ascent of the RGB. The details of this process depend crucially on the precise abundance profile in the H-burning shell (see, e.g., Cassisi, Salaris, & Bono 2002). In the observed CMDs and RGB luminosity functions (LFs) of globular star clusters, and as first predicted by Thomas (1967) and Iben (1968), one in fact identifies the so-called *RGB "bump"* as an observed counterpart of this stellar interior phenomenon (e.g., King, Da Costa, & Demarque 1985; Fusi Pecci et al. 1990). Importantly, the RGB bump also appears to correspond to the position in the CMD that marks the onset of mixing of nuclearly-processed elements beyond that predicted by the canonical theory (e.g., Gratton et al. 2000; Denissenkov & VandenBerg 2003; Charbonnel 2005; Recio-Blanco & de Laverny 2007 and references therein).

To determine the position of the RGB bump in NGC 5286, we construct a smoothed RGB LF, following the procedure described in Zoccali et al. (1999). This already reveals a candidate bump at $V' \simeq 16.4$ (Fig. 8, *upper panel*. To confirm that this is a significant detection, we carry out a power-

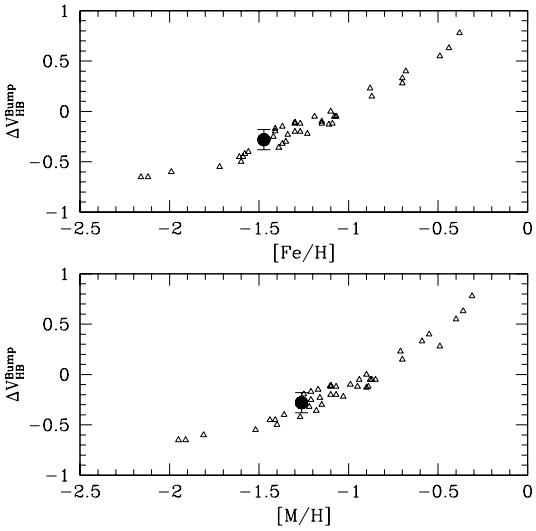


FIG. 9.— Magnitude difference between the bump and the HB, V_{HB}^{bump}, as a function of $[Fe/H]_{CG97}$ (*top*) and [M/H] (*bottom*). The *filled circle* indicates the derived position for NGC 5286, whereas the triangles correspond to data for other globular clusters, from Ferraro et al. (1999).

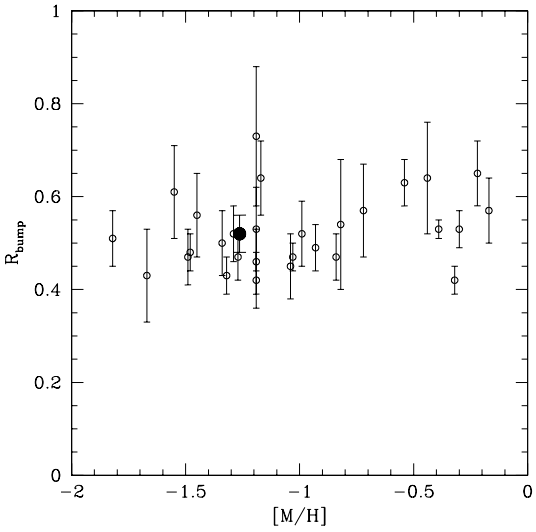


FIG. 10.— R_{bump} vs global metallicity. The *filled circle* indicates the measured value for NGC 5286.

law fit to this LF, which is shown as a dash-dotted gray line in Figure 8. We then calculate the difference between the actual smoothed RGB LF and the power-law fit, and compare the result with the expected 3 – Poisson fluctuation level. As shown in Figure 8 (*middle panel*), the most significant feature in the RGB LF does indeed lie at the position previously suspected to correspond to the RGB bump. We carry out a Gaussian fit to the data within a 0.3 mag range around the detected feature, which leads to the curve shown as a gray line in Figure 8 (*middle panel*). The parameters of the fit are as follows: V_{bump} = 16.415 0.002 mag, $_{bump}$ = 0.093 0.004 mag. We confirm this detection using the integrated RGB LF method of Fusi Pecci et al. (1990) (Figure 8, *bottom panel*), and finally adopt for the position of the bump a value V_{bump} = 16.41 0.05 mag – where the adopted error bar represents a compromise between the width of the Gaussian fit and the formal error in the position of its center.

We next compute the difference in brightness between the RGB bump and the ZAHB level (defined as in §3.2), obtaining V_{HB}^{bump} = –0.28 0.05. A plot showing V_{HB}^{bump} as a function of metallicity is presented in Figure 9. The cluster data are from Table 5 in F99. In this figure, the derived position of NGC 5286 is shown as a filled dot with error bar; as we can see, the position of NGC 5286 in this plane is consistent with our inferred metallicity for the cluster.

We also calculated R_{bump} (Bono et al. 2001), the ratio between the number of RGB stars in the bump region (V_{bump} 0.4) and the number of RGB stars in the interval $V_{bump}+0.5 < V < V_{bump}+1.5$. This quantity is important in revealing whether deep mixing can start prior to the bump level or not. In our case we obtained R_{bump} = 0.52 0.04. Comparision of the measured R_{bump} parameter with the cluster sample of Bono et al. 2001 (their Table 1) shows good agreement, as can be seen from Figure 10. This suggests, as discussed by Bono et al., that an important amount of deep mixing does not take place before stars reach the bump.

4. COMPARISON WITH M3

We compare NGC 5286 with M3, a well studied cluster of similar metallicity ([Fe/H] = –1.57, according to Harris 1996). Figure 11 shows the fiducial points for M3, as derived by us following the same procedure as in §3 for NGC 5286, compared with those for NGC 5286, in the (B–V, V) plane. The M3 photometry was kindly provided by P. B. Stetson (2008, priv. comm.; see also Stetson et al. 2005). VandenBerg et al. (2006) isochrones for [Fe/H] = –1.71, [/Fe] = 0.3, and ages ranging from 8 to 18 Gyr are also shown. We chose the metallicity nearest to the one that we found for NGC 5286 in the ZW84 scale (see §3.2). A variation in the metallicity at the level of the difference between the results in the ZW84 and CG97 is not expected to affect substantially the estimation of relative ages (see, e.g., VandenBerg, Bolte, & Stetson 1990).

As in Stetson et al. (1999), the isochrones and fiducial points for both clusters were shifted horizontally to match each other's turnoff colors (*vertical line*), and then shifted vertically to register the point on the upper MS that lies 0.05 mag redder than the turnoff (*cross*). According to this figure, and on the basis of equation (1) in VandenBerg & Stetson (1990), assuming an identical [O/Fe] = 0.3 for both clusters, NGC 5286 seems to be around 1.7 0.9 Gyr older than M3 – which goes in the right sense to explain the former's bluer HB.

As well known, another method to derive GC ages is the so-called *V method*, which is based on the difference in magnitude between the HB and the TO levels. In this case we follow the procedure described by Chaboyer et al. (1996), using their equation (2) and assuming M_V(RR) = 0.20[Fe/H]+0.98. We decided to use this specific calibration for M_V(RR) because is gives the closest match to the absolute magnitudes of RR Lyrae stars recently calibrated by Catelan & Cortés (2008). To obtain the position of the TO and HB levels for M3, we use the same procedure as for NGC 5286. Then we used V(HB) = V_{ZAHB} – 0.05[Fe/H] – 0.2, again as in Chaboyer et al.. We thus obtained V_{HB}^{TO} = 3.48 0.1 for NGC 5286, and V_{HB}^{TO} = 3.39 0.1 for M3. These values imply that NGC 5286 is around 1.5 1.6 Gyr older than M3, in good agreement with the value previously derived on the basis of the horizontal method.

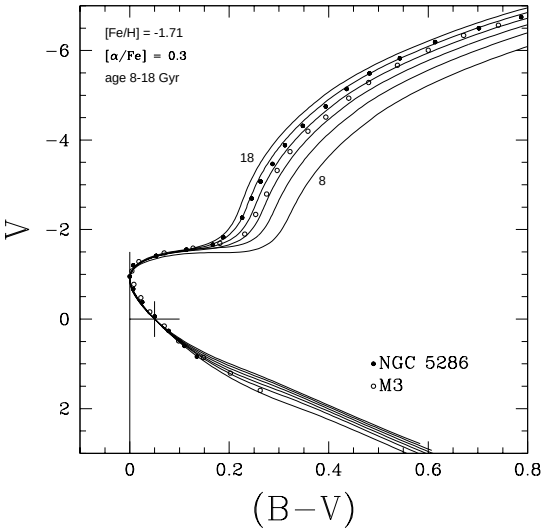


FIG. 11.— Comparision of the M3 (*crosses*) and NGC 5286 (*points*) ridgelines with theoretical isochrones (from VandenBerg et al. 2006) for [Fe=H] = –1.71, [=Fe] = 0.3, and ages ranging from 8 to 18 Gyr, in steps of 2 Gyr (*lines*). The models and data were registered as recommended in Stetson et al. (1999).

We refrain from providing an absolute age for NGC 5286 in this paper, given the well known problems in accurately defining a proper age scale for Galactic globular clusters, but do note that, in case the above results are correct, NGC 5286 may rank among the oldest globulars in our galaxy (compare, for instance, with Table 4 in VandenBerg 2000). This also implies that, if NGC 5286 is a bona fide member of the Canis Major dSph galaxy, then the latter's oldest components may be at least as old as the oldest Milky Way GCs.

5. SUMMARY

We have obtained *BV* CCD photometry for the globular cluster NGC 5286, extending about two magnitudes deeper than the MS turnoff. The latter is found to be aproximately at $V_{TO} = 20.05 \pm 0.1$ mag and $(B-V) = 0.66 \pm 0.02$. We detect the RGB bump at $V_{bump} = 16.41 \pm 0.05$ mag.

A variety of HB morphology parameters was also computed. A metallicity of [Fe=H] = -1.70 ± 0.10 was derived in the ZW84 scale based on several RGB parameters, in good agreement with Harris (1996).

A comparision between the NGC 5286 and M3 CMDs with theoretical isochrones for [Fe=H] = –1.71 and [=Fe] = 0.3 suggests that NGC 5286 is around 1.7 ± 0.9 Gyr older than M3, which goes in the right sense to explain the former's bluer HB morphology. If NGC 5286 is indeed a bona fide member of the Canis Major dSph galaxy, this implies that the latter's oldest components may be at least as old as the oldest Milky Way GCs.

We thank the referee for several constructive comments that led to a significant improvement in the presentation of our results. M. Zorotovic and MC acknowledge support by Proyecto Fondecyt Regular #1071002, M. Zoccali acknowledges support by Proyecto Fondecyt Regular #1085278. HAS was supported by CSCE and NSF grant AST 0607249.

REFERENCES

Bedin, L. R., Piotto, G., Zoccali, M., Stetson, P. B., Saviane, I., Cassisi, S., & Bono, G. 2000, A&A, 363, 159
Bonifacio, P., Monai, S., & Beers, T. C. 2000, AJ, 120, 2065
Bono, G., Cassisi, S., Zoccali, M., & Piotto, G. 2001, AJ, 546, 109
Borissova, J., Ivanov, V. D., Stephens, A. W., Catelan, M., Minniti, D., & Prieto, G. 2007, A&A, 474, 121
Brocato, E., Buonanno, R., Malakhova, Y., & Piersimoni, A. M. 1996, A&A, 311, 778
Buonanno, R. 1993, in The Globular Cluster-Galaxy Connection, ASP Conf. Ser., Vol. 48, ed. G. H. Smith & J. P. Brodie (San Francisco: ASP), 131
Buonanno, R., Corsi, C., Bellazini, M., Ferraro, F. R., & Fusi Pecci, F. 1997 AJ, 113, 706
Carretta, E., & Gratton, R. G. 1997, A&AS, 121, 95 (CG97)
Cassisi, S., Salaris, M., & Bono, G. 2002, ApJS, 565, 1231
Catelan, M. 2005, preprint (astro-ph/0507464)
Catelan, M. 2007, RevMexAA Conf. Ser., 26, 93
Catelan, M., et al. 2006, Mem. Soc. Astron. Italiana, 77, 202
Catelan, M. & Cortés, C. 2008 ApJ, 676L, 135
Clement, C. M., et al. 2001, AJ, 122, 2587
Chaboyer, B., Demarque, P., & Sarajedini, A. 1996, ApJ, 459, 558
Charbonnel, C. 2005, in Cosmic Abundances as Records of Stellar Evolution and Nucleosynthesis, ASP Conf. Ser., Vol. 336, ed. T. G. Barnes III & F. N. Bash (San Francisco: ASP), 119
Contreras, R., Catelan, M., Smith, H. A., Pritzl, B. J., & Borissova, J. 2005, ApJ, 623, L117
Denissenkov, P. A., & VandenBerg, D. A. 2003, ApJ, 593, 509
Ferraro F. R., Messineo, M., Fusi Pecci, F., De Palo, M. A., Straniero, O., Chieffi,A., & Limogni, M. 1999, AJ, 118, 1738
Forbes, D. A., Strader, J., & Brodie, J. P. 2004, AJ, 127, 3394
Frinchaboy, P. M., Majewski, S. R., Crane, J. D., Reid, I. N., Rocha-Pinto, H. J., Phelps, R. L., Patterson, R. J., & Muñoz, R. R. 2004, ApJ, 602, L21
Fusi Pecci, F., Ferraro, F. R., Crocker, D. A., Rood, R. T., & Buonanno, R. 1990, A&A, 238, 95
Gallart, C., Zoccali, M., Bertelli, G., Chiosi, C., Demarque, P., Girardi, L., Nasi, E., Woo, J.-H., Yi, S. 2003, AJ, 125, 742
Gratton, R. G., Sneden, C., Carretta, E., & Bragaglia, A. 2000, A&A, 354, 169
Harris, W. E. 1996, AJ, 112, 1487
Iben, I., Jr. 1968, Nature, 220, 143
King, C. R., Da Costa, G. S., & Demarque, P. 1985, ApJ, 299, 674
Landolt, A. U. 1992, AJ, 104, 340
Lee, Y.-W. 1990, ApJ, 363, 159
Lee, Y.-W., Demarque, P., & Zinn, R. 1990, ApJ, 350, 155
Piotto, G., Zoccali, M., King, I. R., Djorgovski, S. G., Sosin, C., Rich, R. M., & Meylan, G. 1999, AJ, 118, 1727
Preston, G. W., Shectman, S. A. & Beers, T. C. 1991, ApJ, 375, 121
Recio-Blanco, A., & de Laverny, P. 2007, A&A, 461, L13
Reed, B. C., Hesser, J. E., & Shawl, S. J. 1988, PASP, 100, 545
Salaris, M., Chieffi, A., & Straniero, O. 1993, ApJ, 414, 580
Samus, N., Ipatov, A., Smirnov, O., Kravtsov, V., Alcaíno, G., Liller, W., & Alvarado, F. 1995, A&AS, 112, 439
Sarajedini, A. 1994, AJ, 107, 618
Schlegel, D. J., Finkbeiner, D. P., & Davis, M. 1998, ApJ, 500, 525
Stetson, P. B. 1987, PASP, 99, 191
Stetson, P. B. 1994, PASP, 106, 250
Stetson, P. B., Catelan, M., & Smith, H. A. 2005, PASP, 117, 1325
Stetson, P. B., et al. 1999, AJ, 117, 247
Thomas, H.-C. 1967, ZAp, 67, 420
VandenBerg, D. A. 2000, ApJS, 129, 315
VandenBerg, D. A., Bergbusch, P. A., & Dowler, P. D. 2006, ApJS, 162, 375
VandenBerg, D. A., Bolte, M., & Stetson, P. B. 1990, AJ, 100, 445
VandenBerg, D. A., & Stetson, P. B. 1990, AJ, 102, 1043
Webbink, R. F. 1985, in Dynamics of Star Clusters, IAU Symp. 113, ed. J. Goodman & P. Hut (Dordrecht: Reidel), 541
Zinn, R. 1985, ApJ, 493, 424
Zinn, R. 1986, in Stellar Populations, ed. C. A. Norman, A. Renzini, & M. Tosi (Cambridge: Cambridge University Press), 73
Zinn, R. & West, M. J. 1984, ApJS, 55, 45 (ZW84)
Zoccali, M., Cassisi, S., Piotto, G., Bono, G., & Salaris, M. 1999, ApJ, 518, 49